

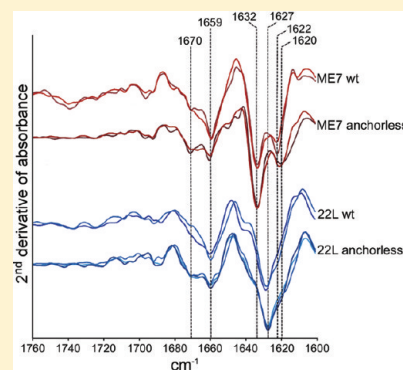
# Effect of Glycans and the Glycophosphatidylinositol Anchor on Strain Dependent Conformations of Scrapie Prion Protein: Improved Purifications and Infrared Spectra

Gerald S. Baron,<sup>\*,†</sup> Andrew G. Hughson,<sup>†</sup> Gregory J. Raymond,<sup>†</sup> Danielle K. Offerdahl,<sup>†</sup> Kelly A. Barton,<sup>†</sup> Lynne D. Raymond,<sup>†</sup> David W. Dorward,<sup>‡</sup> and Byron Caughey<sup>†</sup>

<sup>†</sup>Laboratory of Persistent Viral Diseases and <sup>‡</sup>Microscopy Unit, Research Technology Branch, Rocky Mountain Laboratories, National Institute of Allergy and Infectious Diseases, National Institutes of Health, Hamilton, Montana 59840, United States

**S** Supporting Information

**ABSTRACT:** Mammalian prion diseases involve conversion of normal prion protein, PrP<sup>C</sup>, to a pathological aggregated state (PrP<sup>res</sup>). The three-dimensional structure of PrP<sup>res</sup> is not known, but infrared (IR) spectroscopy has indicated high, strain-dependent  $\beta$ -sheet content. PrP<sup>res</sup> molecules usually contain a glycophosphatidylinositol (GPI) anchor and large Asn-linked glycans, which can also vary with strain. Using IR spectroscopy, we tested the conformational effects of these post-translational modifications by comparing wild-type PrP<sup>res</sup> with GPI- and glycan-deficient PrP<sup>res</sup> produced in GPI-anchorless PrP transgenic mice. These analyses required the development of substantially improved purification protocols. Spectra of both types of PrP<sup>res</sup> revealed conformational differences between the 22L, ME7, and Chandler (RML) murine scrapie strains, most notably in bands attributed to  $\beta$ -sheets. These PrP<sup>res</sup> spectra were also distinct from those of the hamster 263K scrapie strain. Spectra of wild-type and anchorless 22L PrP<sup>res</sup> were nearly indistinguishable. With ME7 PrP<sup>res</sup>, modest differences between the wild-type and anchorless spectra were detected, notably an  $\sim 2\text{ cm}^{-1}$  shift in an apparent  $\beta$ -sheet band. Collectively, the data provide evidence that the glycans and anchor do not grossly affect the strain-specific secondary structures of PrP<sup>res</sup>, at least relative to the differences observed between strains, but can subtly affect turns and certain  $\beta$ -sheet components. Recently reported H–D exchange analyses of anchorless PrP<sup>res</sup> preparations strongly suggested the presence of strain-dependent, solvent-inaccessible  $\beta$ -core structures throughout most of the C-terminal half of PrP<sup>res</sup> molecules, with no remaining  $\alpha$ -helix. Our IR data provide evidence that similar core structures also comprise wild-type PrP<sup>res</sup>.



The structure of the infectious, pathological form of prion protein (PrP<sup>res</sup> or PrP<sup>Sc</sup>) has been an enduring mystery for decades. During the course of transmissible spongiform encephalopathies (TSEs) or mammalian prion diseases, PrP<sup>res</sup> is formed from the host's normal prion protein, PrP<sup>sen</sup> or PrP<sup>C</sup>, in a process that involves oligomerization and massive conformational change. PrP<sup>C</sup> is largely  $\alpha$ -helical and disordered,<sup>1–3</sup> while PrP<sup>res</sup> is an ill-defined, often fibrillar multimer that is rich in  $\beta$ -sheet.<sup>1,4–6</sup> Whereas the three-dimensional structures of different PrP<sup>C</sup> molecules have been determined by solution NMR<sup>7</sup> and X-ray crystallography,<sup>8</sup> detailed structural analyses of PrP<sup>res</sup> have been confounded by its insoluble multimeric properties. Rough secondary structure compositions of PrP<sup>res</sup> have been estimated by infrared (IR)<sup>1,4,5,9</sup> and circular dichroism spectroscopic studies.<sup>6</sup> IR<sup>9–11</sup> and a variety of biochemical measurements<sup>12–20</sup> have also indicated the existence of prion strain-dependent conformations of PrP<sup>res</sup>. Electron crystallography of two-dimensional arrays present in certain PrP<sup>Sc</sup> preparations has given additional low-resolution maps of an apparent nonfibrillar PrP<sup>res</sup> ultrastructure.<sup>21,22</sup> The strain-dependent dimensions of fibrillar PrP<sup>res</sup> ultrastructures have been determined by electron microscopy and atomic force microscopy.<sup>23</sup>

During biosynthesis, PrP<sup>C</sup> is usually modified by the addition of up to two structurally diverse Asn-linked glycans<sup>24,25</sup> and a glycophosphatidylinositol (GPI) anchor.<sup>26</sup> These post-translational modifications are often retained upon conversion of PrP<sup>C</sup> to PrP<sup>res</sup>. One of the well-documented strain-dependent variables in PrP<sup>res</sup> structures is the relative proportion of singly glycosylated, doubly glycosylated, and unglycosylated molecules (i.e., glycoforms) in PrP<sup>res</sup> aggregates from a given source.<sup>12,13,17,18,27</sup> Moreover, studies with transgenic mice or cells expressing PrP<sup>C</sup> mutants lacking one or both of the Asn-linked glycosylation sites have shown striking strain-dependent effects on prion disease susceptibility and pathogenesis.<sup>28–30</sup> Such observations suggest that glycans might modulate PrP<sup>res</sup> conformations or that PrP<sup>res</sup> conformers might vary in their propensities, or abilities, to incorporate differentially glycosylated PrP<sup>C</sup> molecules. There is evidence of the latter possibility from studies of PrP<sup>res</sup> formation *in vitro*<sup>27,31</sup> and in scrapie-infected cells.<sup>32</sup> On the other hand, another report has suggested that glycosylation may not be

**Received:** March 16, 2011

**Revised:** April 17, 2011

**Published:** May 03, 2011



necessary for strain-specific differences in PrP<sup>res</sup> conformation, based on the location of proteinase K digestion sites.<sup>33</sup> In any case, no higher-resolution structural comparisons have been made to directly investigate the impact of glycosylation on PrP<sup>res</sup> conformation for a given strain.

Removing the GPI anchor of PrP can also have dramatic effects on prion disease pathogenesis. Transgenic mice expressing PrP<sup>C</sup> that lacks the C-terminal GPI anchor signal peptide (anchorless PrP<sup>C</sup>) can be infected intracerebrally with prions, but the resulting disease (called fatal transmissible amyloid encephalopathy) is more like a cerebral amyloid angiopathy than a typical TSE disease.<sup>34,35</sup> Interestingly, the absence of GPI-anchored PrP<sup>C</sup> in these mice also nearly eliminates prion neuroinvasion and neural spread from more peripheral sites of inoculation.<sup>36</sup> Anchorless PrP<sup>C</sup> that is expressed in transgenic mice and in cell cultures is deficient in Asn-linked glycans.<sup>34,37</sup> The reason for this is unclear but presumably reflects an important role for membrane anchoring for proper glycosylation during biosynthesis.<sup>38</sup> Consequently, when infected with mouse scrapie prions, these transgenic mice produce PrP<sup>res</sup> that is both lacking the GPI anchor and severely underglycosylated.

The recent availability of anchorless, as well as wild-type, PrP<sup>res</sup> now permits analyses of the influence of glycans and GPI anchors on PrP<sup>res</sup> structures. Because IR spectroscopy is capable of discerning prion strain-dependent variations in PrP<sup>res</sup> secondary structures,<sup>9–11,39</sup> it is probably the best available method for detecting conformational effects of these post-translational modifications on PrP<sup>res</sup> strains. The amide I region (~1600–1700 cm<sup>-1</sup>) of protein IR spectra reflects vibrational absorbances by the amide linkages that comprise the polypeptide backbone. The frequencies of these absorbances are modulated by transition dipole couplings and by hydrogen bonds between backbone amide protons and carbonyl oxygens of different amino acid residues, which, in turn, are determined primarily by various secondary structures. One practical obstacle to comparisons of anchorless and wild-type PrP<sup>res</sup> by IR has been difficulties in obtaining wild-type murine scrapie PrP<sup>res</sup> preparations of sufficient purity. In this study, we describe new improved purification protocols for different strains of anchorless and wild-type PrP<sup>res</sup> and their conformational comparisons by IR spectroscopy.

## EXPERIMENTAL PROCEDURES

**Purification of Detergent-Resistant Membrane (DRM) PrP<sup>res</sup>.** The term detergent-resistant membrane (DRM) PrP<sup>res</sup> refers to the use of brain DRMs as a starting subcellular fraction from which the PrP<sup>res</sup> is subsequently purified. Wild-type PrP<sup>res</sup> was purified from Syrian golden hamsters infected with the 263K scrapie strain or mice infected with the 22L or ME7 scrapie strain. Brains were dissected from animals exhibiting clinical scrapie signs, rinsed in PBS, blotted on filter paper to remove excess blood, snap-frozen in liquid nitrogen, and stored at -80 °C until they were needed. To isolate DRM PrP<sup>res</sup>, brains were first thawed and rinsed in cold CBS [20 mM citrate and 137 mM NaCl (pH 6.0)]. A 10% brain homogenate was then prepared from ~2 g of tissue by Dounce homogenization in CBS. In certain preparations, the homogenate was centrifuged at 1000g for 5 min at 4 °C to remove large insoluble material. The supernatant was then subjected to Brij-96 (Fluka) extraction as described below. This optional centrifugation step had no noticeable effect on the purity of the final product or on the IR

spectra of DRM PrP<sup>res</sup> (data not shown) but could reduce the yield of DRM PrP<sup>res</sup> depending on the strain. The reduced yield was due to unexpected localization of the majority of the PrP<sup>res</sup> to the 1000g pellet fraction for certain strains such as 22L (data not shown). Therefore, we recommend either omitting this centrifugation step or analyzing the partitioning of PrP<sup>res</sup> and optimizing Brij-96 extraction conditions for strains not described here. The homogenate was rapidly and thoroughly mixed on ice with 1 volume of ice-cold 1% Brij-96 (in CBS) and incubated on a rotisserie at 4 °C for 30 min. After Brij-96 extraction, the sample was adjusted to 26% OptiPrep [in 10 mM citrate and 137 mM NaCl (pH 6.0)] and split equally across six prechilled centrifuge tubes. This fraction was overlaid with layers of 23% (12 mL) and 8% (8 mL) OptiPrep [in 10 mM citrate and 137 mM NaCl (pH 6.0)] followed by 1 mL of 10 mM citrate and 137 mM NaCl (pH 6.0). The gradients were centrifuged in a prechilled Beckman SW32 rotor at 18500 rpm for 2 h at 4 °C. Prominent lipid bands were visible at the CBS–8% OptiPrep and 8%–23% OptiPrep interfaces, the latter representing the PrP<sup>res</sup>-enriched fraction. The layers above the 8%–23% lipid band were carefully aspirated and discarded prior to careful collection of the lipid band at the 8%–23% interface, which we term the DRM fraction.

The second portion of the procedure involved extraction and purification of PrP<sup>res</sup> from the DRM fraction. After equilibration of the sample to room temperature (RT), we performed a high-salt extraction on the DRM fraction by adding 1/2 volume of 5 M NaCl [in 0.15 M Tris (pH 8.0)], mixing thoroughly, and incubating the sample for 15 min at RT. The high-salt-washed DRMs were split into four tubes and fractionated on a second floatation gradient consisting of a bottom fraction of salt-extracted DRMs adjusted to 26% OptiPrep (from a 60% stock) and overlaid with ~1/4 volume (~7 mL) of 23% OptiPrep in TBS [10 mM Tris and 137 mM NaCl (pH 8.0)] and 1 mL of TBS. The gradients were centrifuged in an SW32 rotor at 18500 rpm for 2 h at 20 °C. This high-salt extraction was intended to disrupt electrostatic interactions between PrP<sup>res</sup> and high-molecular mass molecules such as glycosaminoglycans and ferritin<sup>40</sup> and remove some of these contaminants from the DRMs. The lipid band at the TBS–23% OptiPrep interface was carefully collected and adjusted to a final volume of 27 mL with TBS. To solubilize the membranes and digest nucleic acids, 3 mL of a 20% sarkosyl/0.5 M Tris mixture (pH 7.5) was added followed by Benzonase to a final concentration of 25 units/mL and incubation at 37 °C for 30 min. The sample was then digested with 10 µg/mL PK for 1 h at 37 °C. PK digestion was terminated by addition of Pefabloc SC (final concentration of 2 mM) and incubation on ice for 15 min. To remove PK, the sample was first adjusted to 30 mM EDTA and incubated for 5 min at RT. Next, the sample was centrifuged at 1000g for 5 min at RT to remove large insoluble material. The supernatant was adjusted to contain a final NaCl concentration of 1.8 M, and the entire mixture was gently overlaid onto 1/2 volume of a sucrose pad solution [1 M sucrose, 0.1 M NaCl, 0.5% sulfobetaine 3-14, and 10 mM Tris (pH 7.5)]. After centrifugation in a Beckman Type 50.2 Ti rotor at 45000 rpm for 2 h at 20 °C, the supernatant was carefully removed without disturbing the pellet. The pellet was washed by resuspension in 3 mL of 0.5% sulfobetaine (in PBS) followed by centrifugation in a TLA100.3 rotor at 70000 rpm for 30 min at 4 °C. The supernatant was thoroughly removed, and the final DRM PrP<sup>res</sup> pellet was resuspended in 0.5% sulfobetaine (in PBS) by pipetting and brief cuphorn sonication as needed. Yields of DRM PrP<sup>res</sup> ranged from ~2.5



to 12.5  $\mu\text{g/g}$  of brain for 22L and ME7 strains and from  $\sim 25$  to 50  $\mu\text{g/g}$  of brain for 263K with the lower yields corresponding to preparations with homogenates subjected to the optional 1000g clearing step described above.

**Purification of Anchorless PrP<sup>res</sup>.** Brain homogenates from scrapie-infected tg44<sup>+/+</sup> transgenic mice<sup>35</sup> expressing GPI anchorless PrP<sup>C</sup> were adjusted to contain 50 mM Tris, 137 mM NaCl, and 2% sarkosyl (pH 8.0) (TBSS) and incubated for 20 min at RT. After Benzonase treatment (25 units/mL, 30 min) to digest nucleic acids, the samples were centrifuged (Beckman Type 50.2 Ti rotor, 24 min,  $\sim 40500g_{\text{max}}$ ) to pellet the PrP<sup>res</sup> and other detergent-insoluble material. These centrifugation conditions provided a  $k$  factor comparable to centrifugation at top speed in a Beckman microcentrifuge. The pellet was resuspended in TBSS, carefully avoiding the brown portion of the pellet. The sample was then digested with proteinase K (PK) at 10  $\mu\text{g/mL}$  for 1 h. After termination of the PK digest, a PK-stripping procedure similar to that described previously<sup>41</sup> was performed by addition of EDTA (final concentration of 30 mM) and NaCl (final concentration of 1.7 M), layering onto a sucrose cushion [1 M sucrose, 100 mM NaCl, 0.5% sulfobetaine 3-14, and 10 mM Tris (pH 7.4)], and recovery of the PrP<sup>res</sup> by centrifugation as described above through the sucrose cushion. The pellet was then resuspended in 0.5% sulfobetaine 3-14 (in PBS) and centrifuged again to wash the pellet. The final PrP<sup>res</sup> pellet was resuspended in a small volume of 0.5% sulfobetaine 3-14 (in PBS) with brief cuphorn sonication. The yields of anchorless PrP<sup>res</sup> were  $\sim 168 \mu\text{g/g}$  of brain for 22L,  $\sim 123 \mu\text{g/g}$  of brain for Chandler (RML), and  $\sim 75 \mu\text{g/g}$  of brain for ME7. Control “mock” preparations from age-matched uninfected mice contained a small pellet of translucent material that was resuspended as described for the anchorless PrP<sup>res</sup> pellets. A more detailed description of the purification procedure for anchorless PrP<sup>res</sup> can be found elsewhere.<sup>42</sup>

**Sodium Dodecyl Sulfate–Polyacrylamide Gel Electrophoresis (SDS–PAGE) and Immunoblotting.** Samples were denatured by being boiled for 8–10 min in sample buffer [4 M urea, 5% SDS, 5% glycerol, 3 mM EDTA, 0.02% bromophenol blue, and 62.5 mM Tris (pH 6.8)] with either DTT (50 mM) or  $\beta$ -mercaptoethanol (4%) as a reducing agent. As needed, samples were cuphorn sonicated in sample buffer to improve solubilization of highly stable protein aggregates. Proteins were separated on 10% Bis-Tris NuPAGE gels in MES running buffer. GelCode Blue staining was performed following the manufacturer’s recommendations (Thermo Scientific). Silver staining was performed as described elsewhere.<sup>43</sup> Purified mouse ferritin was purchased from Lee Biosolutions. The 90–231 fragment of hamster PrP (recPrP<sup>sen</sup> 90–231) (predicted molecular mass of 16243 Da) was purified from *Escherichia coli* as described elsewhere<sup>44</sup> and used as a standard for quantitation of PK-treated anchorless PrP<sup>res</sup>. For immunoblotting, proteins were transferred to PVDF membranes by a semidry method. For PrP immunoblots, prior to blocking, the membranes were treated with either 0.2 M NaOH (30 min) or 3 M GdnSCN (10 min) followed by four rinses with TBS. Primary antibodies used for PrP detection included 6D11 (Covance Research Products) and R20 (rabbit polyclonal antiserum against PrP residues 218–232). Primary antibodies for detecting ferritin included chicken anti-mouse ferritin (Immunology Consultants Laboratory) and rabbit anti-heavy chain human ferritin (Abcam #16875). Secondary antibodies were purchased from Jackson ImmunoResearch (alkaline phosphatase conjugates) or Invitrogen (Alexa Fluor 488 conjugates). Alkaline phosphatase conjugates were detected using Attophos substrate (Promega). Alexa Fluor 488 conjugates were visualized

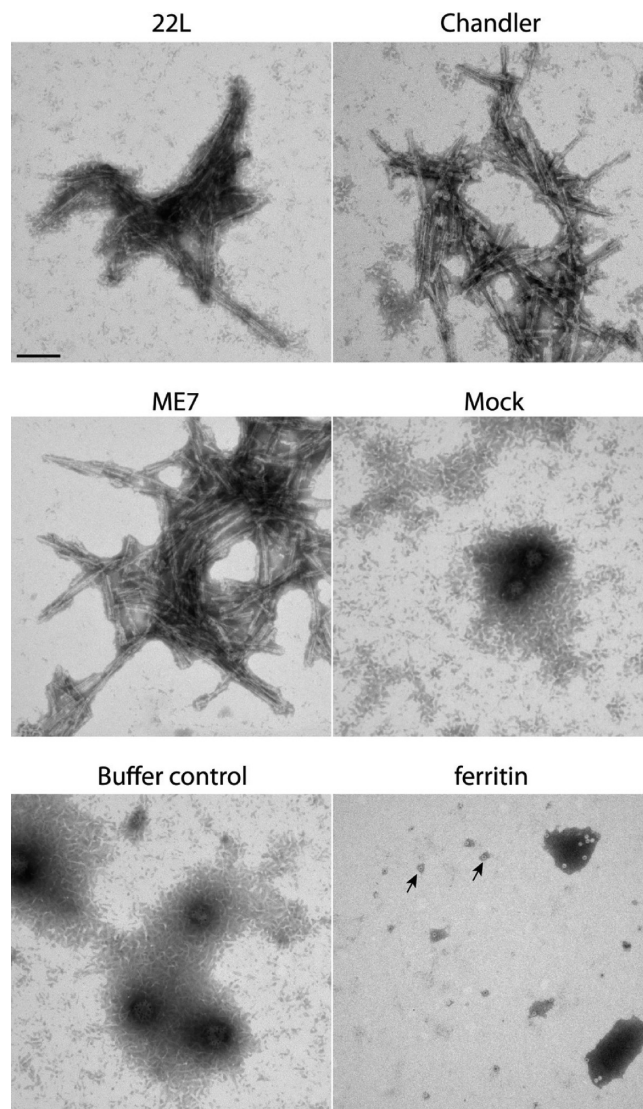


**Figure 1.** Ultrastructure of anchorless PrP<sup>res</sup> fibrils. Samples were stained with methylamine tungstate and examined by TEM. Images of mock anchorless PrP<sup>res</sup>, buffer, and purified mouse ferritin are shown as controls. Arrows denote ferritin particles. The bar is 100 nm.

by direct fluorescence. All blots were imaged on either a Storm or Typhoon scanner (GE Healthcare).

**Transmission Electron Microscopy.** Samples were spotted onto Formvar and carbon-coated grids from Ted Pella (Redding, CA). For samples in Figure 1, grids were freshly glow-discharged. After allowing 30–60 min for adsorption, we washed the grids extensively with ultrapure water. The samples were then stained with either 1% methylamine tungstate (Nano-W from Nanoprobes, Yaphank, NY) or 1% ammonium molybdate where indicated. After drying, the samples were imaged at 80 kV on a Hitachi H7500 electron microscope equipped with an AMT XR-100 digital camera.

**IR Spectroscopy.** IR spectra were recorded using a Perkin-Elmer Spectrum 100 instrument equipped with a diamond attenuated total reflectance sample unit and an MCT detector as described previously.<sup>42</sup> Briefly, PrP<sup>res</sup> aggregates in 0.5% sulfobetaine in PBS containing between 6 and 20  $\mu\text{g}$  of protein were pelleted, washed with water, and resuspended as a 1–2  $\mu\text{L}$  slurry. The slurry was applied to the diamond and dried to a film over a few

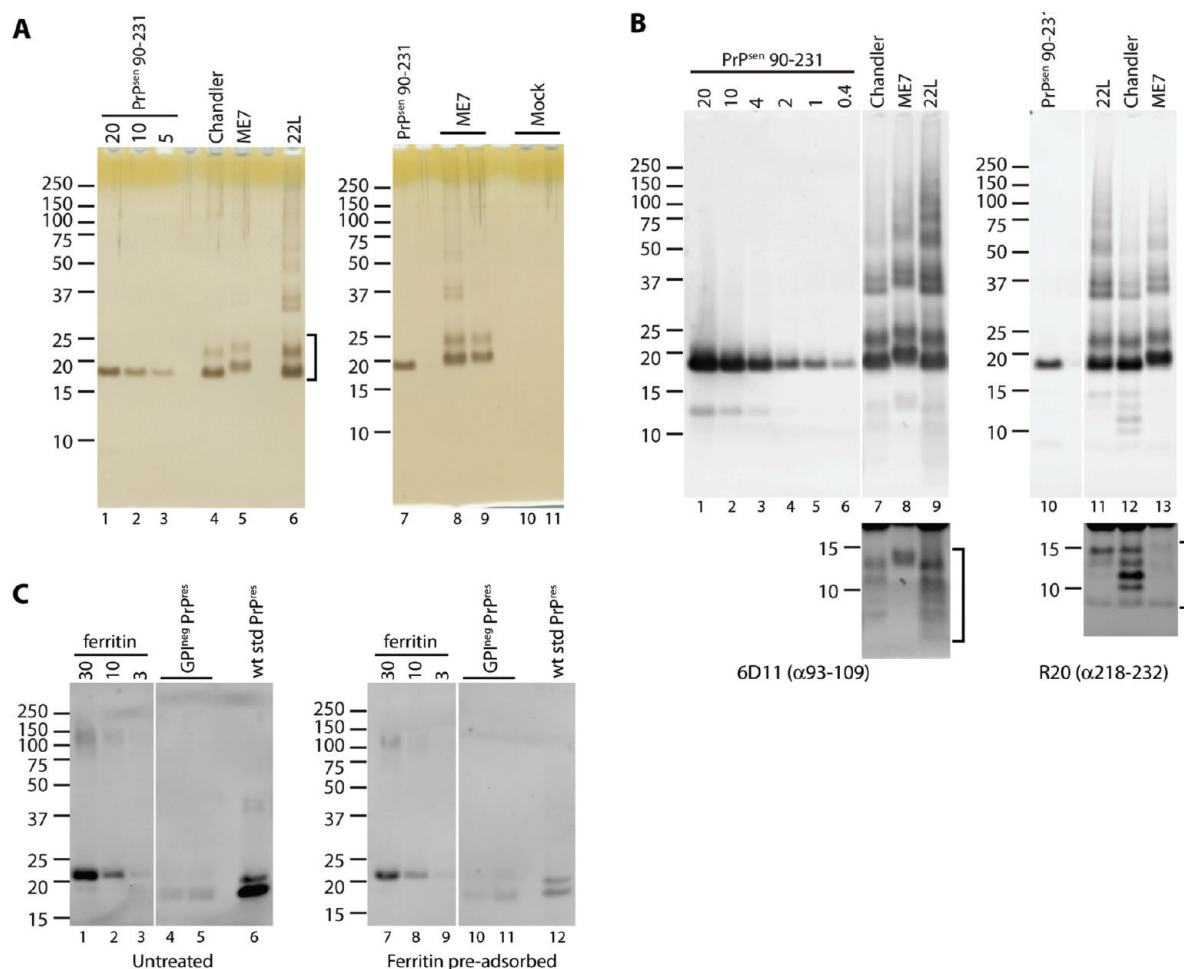


**Figure 2.** Biochemical characterization of anchorless PrP<sup>res</sup> preparations. (A) Silver-stained SDS–PAGE gels. Varying amounts of hamster rPrP<sup>sen</sup> 90–231 (nanograms) were loaded as indicated (lanes 1–3). Lanes 8–11 each contained samples from independent preparations. The bracket indicates bands corresponding to anchorless PrP<sup>res</sup> monomers. (B) Immunoblot analysis with 6D11 or R20 anti-PrP antibodies. Varying amounts of hamster rPrP<sup>sen</sup> 90–231 (nanograms) were loaded as indicated (lanes 1–6). Brackets (bottom panels) indicate strain-specific low-molecular mass species. (C) Immunoblot with the anti-heavy chain ferritin antibody. Blots were performed using antibody without (Untreated) or with (Ferritin pre-adsorbed) preadsorption with purified mouse ferritin to determine ferritin-specific antibody binding. Varying amounts of purified mouse liver ferritin (nanograms) were loaded as indicated (lanes 1–3 and 7–9). GPI<sup>neg</sup> PrP<sup>res</sup>, two independent preparations of anchorless 22L PrP<sup>res</sup> containing either 1.2 (lanes 4 and 10) or 2 μg of PrP<sup>res</sup> (lanes 5 and 11). wt std PrP<sup>res</sup>, 300 ng of wild-type 22L PrP<sup>res</sup> prepared by a standard method.<sup>41</sup> For panels A–C, molecular mass standards are indicated on the left (kilodaltons) and white lines indicate removal of irrelevant lanes.

minutes while the disappearance of the broad liquid water band was followed at  $\sim 1636\text{ cm}^{-1}$  and the appearance of the protein amide I and amide II bands was followed. The spectra were background-subtracted and comprised of 64 accumulations ( $4\text{ cm}^{-1}$  resolution,  $1\text{ cm/s}$  OPD velocity, strong apodization). Those shown were collected as soon as successively collected spectra (each taking 80 s) stabilized, indicating little further evaporation of liquid water. This approach was taken to essentially eliminate spectral contributions from free liquid water without desiccating the protein film any more than necessary. Second-derivative spectra were calculated using the instrument software and 13 data points.

## RESULTS

**Purification of Anchorless PrP<sup>res</sup>.** PrP<sup>res</sup> accumulates in extra-neuronal tissues in scrapie-infected tg44<sup>+/+</sup> transgenic mice expressing anchorless PrP.<sup>45</sup> This provided several potential sources of tissue to use for the purification of anchorless PrP<sup>res</sup>. To identify the optimal

tissue for purification, we first used semiquantitative immunoblotting to compare the levels of PrP<sup>res</sup> in a selection of tissues reported to have the largest amounts of PrP<sup>res</sup>.<sup>45</sup> When samples were normalized for total protein, brain and brown fat contained the highest reproducible levels of PrP<sup>res</sup> (data not shown). Because there is more brain tissue available per animal than brown fat, brain contained the largest total amount of PrP<sup>res</sup> and was therefore chosen as the starting material.

The purification procedure used for anchorless PrP<sup>res</sup> preparations analyzed in this study was based on methods previously described for purification of wild-type<sup>41</sup> and anchorless<sup>23</sup> PrP<sup>res</sup> with some important modifications as detailed in Experimental Procedures. Anchorless PrP<sup>res</sup> was prepared from the brains of tg44<sup>+/+</sup> mice infected with the Chandler (RML), 22L, or ME7 strain of mouse scrapie. Analysis of the samples by transmission electron microscopy (TEM) showed that the PrP<sup>res</sup> preparations were almost exclusively comprised of amyloid-like fibrils (Figure 1) as expected from previous studies,<sup>23,34</sup> the exception being rare





individual collagen fibers that were detected only with extensive searches of entire grids (data not shown). Collagen fibers were also present but infrequent in control mock PrP<sup>res</sup> preparations from age-matched, uninfected tg44<sup>+/+</sup> mice (data not shown). Occasional clusters of electron dense particles were observed in mock and scrapie PrP<sup>res</sup> preparations. Because these were also present in buffer control samples, they were attributed to buffer components such as sulfobetaine (Figure 1, Buffer control). Extensive searches of anchorless and mock anchorless PrP<sup>res</sup> samples failed to detect ferritin, a known contaminant of wild-type PrP<sup>res</sup> preparations<sup>41,46</sup> readily distinguished by its characteristic “fish-eye” appearance (Figure 1). Together, these observations established that the anchorless PrP<sup>res</sup> preparations were highly enriched for amyloid-like fibrils.

Anchorless PrP<sup>res</sup> preparations were further subjected to biochemical analyses to assess sample purity. Analysis by SDS–PAGE with silver staining showed that all anchorless scrapie PrP<sup>res</sup> preparations were highly pure (Figure 2A, lanes 4–6). As previously reported,<sup>34</sup> predominantly unglycosylated PrP was present accompanied by a lower level of monoglycosylated PrP (Figure 2A, lanes 4–6, bracket). Interestingly, anchorless ME7 PrP<sup>res</sup> exhibited a higher apparent molecular mass than Chandler and 22L PrP<sup>res</sup>, suggesting anchorless ME7 PrP<sup>res</sup> contains a larger PK-resistant core. This is consistent with data from mass spectrometric analysis.<sup>42</sup> The bands present in anchorless PrP<sup>res</sup> preparations were specific to scrapie-infected animals as shown by analysis of control mock preparations (Figure 2A, lanes 10 and 11). Ladders of higher-molecular mass species observed by silver staining correlated with bands detected by immunoblotting with two different anti-PrP antibodies (Figure 2B, lanes 7–9 and 11–13), showing that the bands detected by silver staining primarily consist of SDS-resistant oligomers of anchorless PrP<sup>res</sup>. In higher-exposure images, low-molecular mass bands were also visualized that were unique to each strain and antibody, thereby revealing further strain-specific differences between the various anchorless PrP<sup>res</sup> aggregates (Figure 2B, brackets, bottom panels). By comparison with rPrP<sup>sen</sup> 90–231 standards, we estimated the typical yields of anchorless PrP<sup>res</sup> to be ~168 µg/g of brain for 22L, ~123 µg/g of brain for Chandler, and ~75 µg/g of brain for ME7.

Immunoblotting with an anti-heavy chain ferritin antibody was used to more sensitively assay for the presence of ferritin. Ferritin was readily detected in a standard wild-type 22L PrP<sup>res</sup> preparation (Figure 2C, lane 6). However, even when the gel was overloaded with ~4–7-fold more anchorless PrP<sup>res</sup> (~1.2–2 µg) versus the wild type (300 ng), only a faint pair of bands were detected in two independent anchorless PrP<sup>res</sup> preparations (Figure 2C). Similar results were obtained using a different anti-ferritin antibody, chicken anti-mouse ferritin (data not shown). Given the bands precisely comigrate with anchorless PrP<sup>res</sup> monomers and the signal was not competed in a control immunoblot using the anti-ferritin antibody preadsorbed with purified ferritin (Figure 2C, compare lanes 4 and 5 with lanes 10 and 11), these data show there is at most a negligible concentration of ferritin present in anchorless PrP<sup>res</sup> preparations. Altogether, these data establish the very high purity of the anchorless PrP<sup>res</sup> preparations and allow their use in IR spectroscopy studies.

**Purification of Wild-Type PrP<sup>res</sup> from Detergent-Resistant Membranes.** To develop an improved protocol for purification of wild-type PrP<sup>res</sup>, we investigated potential sources for molecules that are co-enriched with PrP<sup>res</sup> in our standard preparation method<sup>41</sup> due to properties shared with PrP<sup>res</sup>

(i.e., detergent insolubility, protease resistance, and high density). Key insight was obtained from characterization of mock PrP<sup>res</sup> preparations derived from uninfected, wild-type animals analogous to the mock preparations from anchorless mice described above. First, ferritin-like particles were detected by electron microscopy (Figure S1A of the Supporting Information) in a manner independent of whether preparations were conducted with or without an optional PK treatment<sup>41</sup> during the preparation. Amorphous objects were also present but less frequent in PK-treated preparations (data not shown). Ferritin contamination was confirmed in mock, 22L, and 263K PrP<sup>res</sup> preparations by immunoblotting with the anti-ferritin antibody (Figure S1B of the Supporting Information). These data are consistent with independent studies.<sup>40,46</sup> In addition to ferritin, other lower-molecular mass proteins were detected in the standard mock PrP<sup>res</sup> by GelCode Blue staining (Figure S1C of the Supporting Information) and silver staining (see below) with apparent molecular masses similar to those of proteins in scrapie PrP<sup>res</sup> preparations that did not correspond to known PrP bands (see below). This indicated that several endogenous brain proteins can contribute to contamination of PrP<sup>res</sup> preparations on the basis of their inherent similarity to the biochemical and biophysical properties of PrP<sup>res</sup>. This finding was supported by independent mass spectrometry studies.<sup>46</sup>

This prompted us to identify biochemical features that might distinguish PrP<sup>res</sup> from the mock PrP<sup>res</sup> contaminants. We determined that the predominant mock PrP<sup>res</sup> proteins lacked N-glycosylation and GPI anchors by digestion with PNGase F and phosphatidylinositol-specific phospholipase C (data not shown). Because PrP<sup>res</sup> is GPI-anchored and associated with brain detergent-resistant membranes (DRMs) for multiple rodent scrapie strains (refs 47–50 and unpublished observations of G. Baron), this suggested that DRM fractionation could be used to separate PrP<sup>res</sup> from many contaminants in PrP<sup>res</sup> preparations and thus generate PrP<sup>res</sup> preparations that are more pure.

Many factors such as the type of detergent, the detergent concentration, the extraction temperature, and the detergent: protein ratio can all influence the association of proteins with DRMs.<sup>51,52</sup> Therefore, we tested two different detergents (Triton X-100 and Brij-96) and various extraction conditions and gradient profiles to optimize enrichment of PrP<sup>res</sup> in DRMs. Although both detergents gave similar results, extraction with cold 0.5% Brij-96 produced slightly better results in small scale experiments (data not shown). As shown in Figure 3A, DRM fractionation of brains from 263K-affected hamsters and 22L-affected mice led to floatation of virtually all PrP<sup>res</sup> in a lipid band of intermediate density consistent with DRMs (fractions 5 and 6). The distribution of total PrP in such gradients, as determined by immunoblotting samples without PK digestion, was identical to that of PrP<sup>res</sup> (data not shown). A lower-density lipid band corresponding to fractions 2 and 3 was also observed, but this did not contain detectable PrP<sup>res</sup>. This membrane fraction may in part be derived from myelin membranes, which can exhibit some detergent resistance.<sup>53</sup> A BCA protein assay of fractions from DRM floatation gradients showed that a substantial portion of the total protein was localized to the higher-density bottom fractions with a much smaller amount corresponding to PrP<sup>res</sup>-containing DRM fractions (Figure 3A, graph). These data established that DRM fractionation led to a significant enrichment of PrP<sup>res</sup> over other brain proteins and biomolecules.

Because DRM fractionation alone would be insufficient to purify PrP<sup>res</sup>, we designed a new purification procedure (described in

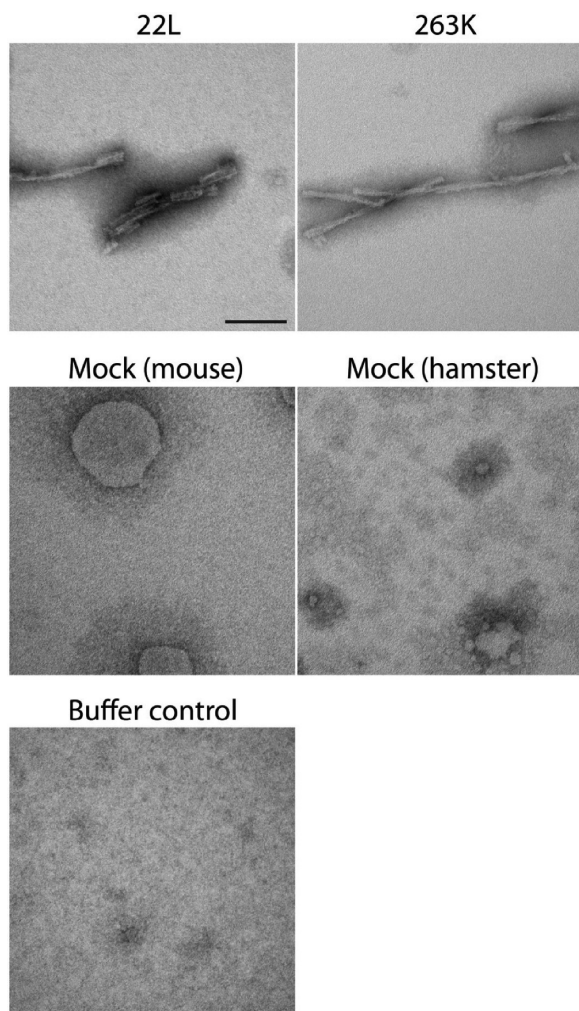


**Figure 4.** Ultrastructure of wild-type DRM PrP<sup>res</sup> fibrils. Samples were stained with ammonium molybdate and examined by TEM. Grids of mock DRM PrP<sup>res</sup> from mice or hamsters were exposed to 10-fold more brain equivalents than 263K or 22L PrP<sup>res</sup> grids to compensate for the extremely low levels of material in mock DRM PrP<sup>res</sup> samples. The bar is 100 nm.

Experimental Procedures) that incorporated DRM fractionation with elements of a standard PrP<sup>res</sup> preparation method.<sup>41</sup> For the sake of simplicity, we refer to preparations using this new method as DRM PrP<sup>res</sup>. Silver stain SDS–PAGE analysis of DRM PrP<sup>res</sup> preparations corresponding to the 263K, 22L, and ME7 scrapie strains showed dramatically reduced levels of the low-molecular mass contaminants present in standard PrP<sup>res</sup> preparations and standard mock PrP<sup>res</sup> preparations (Figure 3B, brackets and arrows). Interestingly, a pellet of material is obtained in mock DRM PrP<sup>res</sup> preparations. However, mock DRM PrP<sup>res</sup> preparations essentially lacked any detectable proteins as compared with equal brain equivalents of standard mock PrP<sup>res</sup> preparations (in Figure 3B, compare lane 3 vs lane 4 and lane 7 vs lane 8). Mock DRM PrP<sup>res</sup> preparations are not devoid of protein as proteins can be detected in these preparations by loading much larger (~5–10-fold more) amounts, but the banding profile still differs from those in standard mock PrP<sup>res</sup> preparations (data not shown). Although the molecular composition of the mock DRM PrP<sup>res</sup> fraction remains to be determined, our data (here and see below) suggest

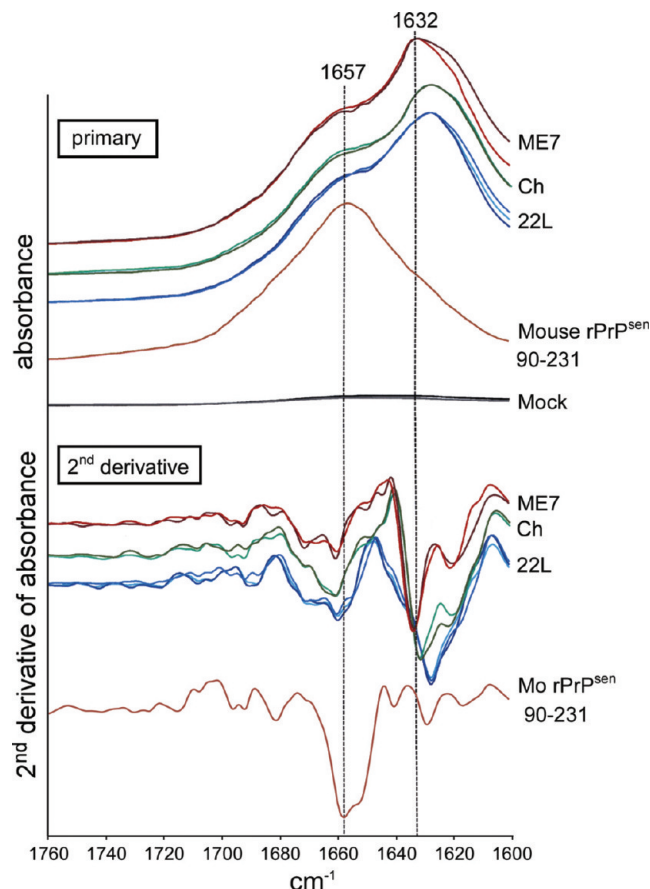


**Figure 5.** IR spectra of anchorless PrP<sup>res</sup> (murine ME7, Chandler, and 22L strains) and recombinant PrP<sup>sen</sup> 90–231. Individual primary (top) and second-derivative (bottom) IR spectra represent independent preparations. For comparison, a spectrum of comparable brain equivalents of a mock anchorless PrP<sup>res</sup> preparation from normal brain tissue is shown. The spectra of the PrP<sup>res</sup> preparations have been normalized to one another so that the absorbance terms are arbitrary. The Chandler spectra are the same as those presented elsewhere in a different context as Supplemental Data.<sup>42</sup>

it may contain lipids. Immunoblot analysis of DRM PrP<sup>res</sup> preparations with an anti-PrP antibody showed a strong correspondence between immunoreactive bands and bands detected by silver staining, including those of both monomeric (arrows) and SDS-resistant oligomeric (brackets) PrP (Figure 3C). The level of ferritin contamination of DRM PrP<sup>res</sup> preparations was also dramatically reduced compared to that of standard PrP<sup>res</sup> preparations as shown in Figure 3D. Although ferritin could be readily detected by immunoblot analysis of standard 263K PrP<sup>res</sup> (arrow), it was undetectable in a similar amount of 263K DRM PrP<sup>res</sup>. Semiquantitative analysis of ferritin content in 22L DRM PrP<sup>res</sup> using two different anti-ferritin antibodies and ferritin standard curves estimated ferritin levels to be ~4.1 or 6.4 ng of ferritin/150 ng of PrP (lane 6 in Figure 3E and Figure S2 of the Supporting Information). By contrast, a standard 22L PrP<sup>res</sup> preparation contained either 78 or 26 ng of ferritin/150 ng of PrP depending upon the antibody used (lane 5 in Figure 3E and Figure S2 of the Supporting Information). This corresponds to a 4.1–19-fold reduction in ferritin content. Because the DRM PrP<sup>res</sup> preparations were treated with PK, we conducted control experiments to confirm that, as expected, pretreating ferritin with PK digestion



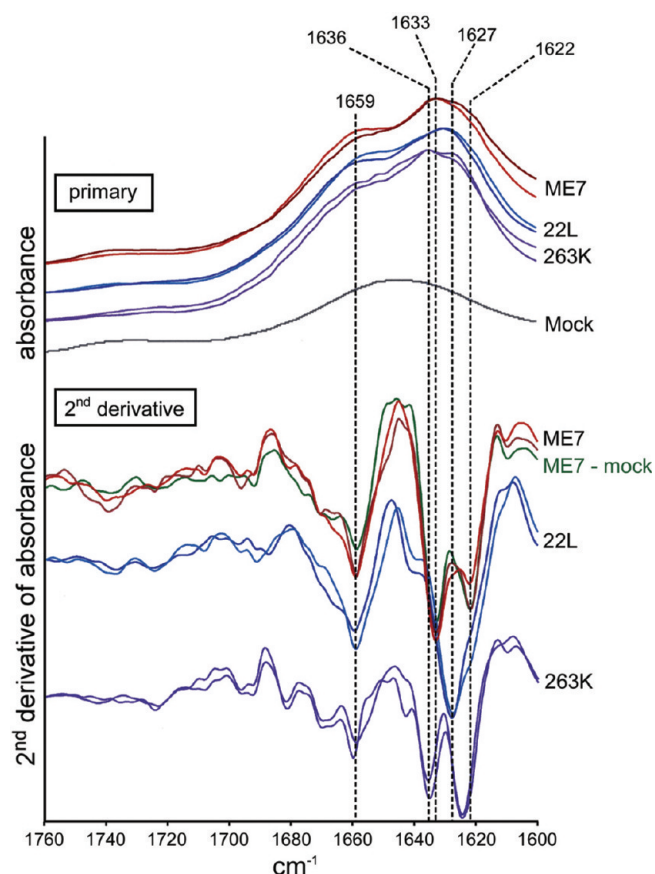


**Figure 6.** IR spectra of wild-type  $\text{PrP}^{\text{res}}$  (mouse ME7 and 22L and hamster 263K strains). Individual primary (top) and second-derivative (bottom) spectra represent independent preparations. A comparable brain equivalent of a mock wild-type  $\text{PrP}^{\text{res}}$  preparation from normal brain tissue is shown as well as a second-derivative spectrum calculated from an ME7-mock difference spectrum (green). Compared to the  $\text{PrP}^{\text{res}}$  spectra, the mock spectrum also displayed a much reduced relative absorbance in the protein amide II region [ $\sim 1545\text{ cm}^{-1}$  (not shown)], suggesting that the absorbance at  $\sim 1650\text{ cm}^{-1}$  is due predominantly to something other than protein. The spectra of the  $\text{PrP}^{\text{res}}$  preparations have been normalized to one another so that the absorbance terms are arbitrary.

had a negligible effect on ferritin detection (lanes 1–4 vs lanes 7–10 in Figure 3E and Figure S2 of the Supporting Information). TEM analysis of DRM  $\text{PrP}^{\text{res}}$  preparations showed they consisted of amyloid-like fibrils with rare collagen fibrils as seen with the anchorless  $\text{PrP}^{\text{res}}$  samples (Figure 4). The amyloid-like fibrils were absent from control mock DRM  $\text{PrP}^{\text{res}}$  preparations, which contained only rare collagen fibrils and vesicle-like structures and were detected only by loading 10 times the sample equivalents versus the 263K or 22L DRM  $\text{PrP}^{\text{res}}$  (Figure 4). Collectively, these observations provide strong evidence that the DRM  $\text{PrP}^{\text{res}}$  purification procedure was successful in generating sufficient yields of highly purified  $\text{PrP}^{\text{res}}$  well-suited for IR spectroscopy and other applications.

**IR Spectra of Anchorless  $\text{PrP}^{\text{res}}$ .** IR spectra of multiple (at least two) independent 22L, ME7, and Chandler anchorless  $\text{PrP}^{\text{res}}$  preparations were compared to one another as well as to spectra of recombinant murine  $\text{PrP}^{\text{sen}}$  90–231 and mock anchorless  $\text{PrP}^{\text{res}}$  preparations from uninfected  $\text{tg44}^{+/+}$  mice. The upper half of Figure 5 shows the primary IR spectra and the bottom the

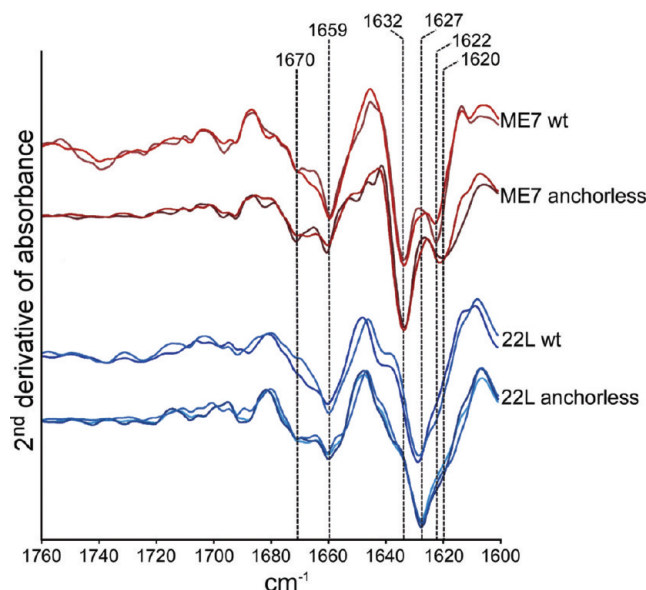


**Figure 7.** Comparisons of anchorless and wild-type  $\text{PrP}^{\text{res}}$  second-derivative IR spectra.

second-derivative spectra calculated directly from the primary spectra. The second derivatives give negative peaks corresponding to maxima in the primary spectra and provide an unbiased enhancement of band resolution. Consistent with previously reported IR spectra of hamster<sup>4,9–11</sup> and murine  $\text{PrP}^{\text{res}}$  preparations,<sup>54</sup> the most prominent absorptions were in a spectral region typically assigned to  $\beta$ -sheets, i.e.,  $1615\text{--}1636\text{ cm}^{-1}$ , indicating predominant  $\beta$ -sheet content. This high  $\beta$ -sheet absorbance was in striking contrast to the predominant absorbance maxima at  $\sim 1657$  and  $1650\text{ cm}^{-1}$  of  $\text{rPrP}^{\text{sen}}$  90–231. The latter maxima were consistent with  $\text{PrP}^{\text{sen}}$ 's high content of  $\alpha$ -helical and disordered secondary structures<sup>2</sup> and previously reported IR data.<sup>1,55</sup> As reported previously for wild-type  $\text{PrP}^{\text{res}}$  from hamsters<sup>4,9–11</sup> and mice,<sup>54</sup> clear differences were observed between the different mouse strains of anchorless  $\text{PrP}^{\text{res}}$ , most notably in the  $\beta$ -sheet region of the second-derivative spectra. These results provide direct evidence that strain-dependent differences in  $\text{PrP}^{\text{res}}$  secondary structure exist in the absence of GPI anchors and, for the most part, N-linked glycans.

**Comparisons of Anchorless and Wild-Type  $\text{PrP}^{\text{res}}$ .** To investigate whether glycans and anchors modify the secondary structures of  $\text{PrP}^{\text{res}}$ , we also recorded IR spectra of fully glycosylated and GPI-anchored wild-type DRM  $\text{PrP}^{\text{res}}$  of the 22L and ME7 strains prepared by the improved purification protocol described above. In addition, an analogous mock preparation from uninfected mouse brain tissue was also analyzed. As shown in Figure 6, the mock preparation gave a spectrum in the  $1600\text{--}1700\text{ cm}^{-1}$  region that was considerably less intense than the corresponding  $\text{PrP}^{\text{res}}$  spectra. Moreover, the mock spectrum was broad and relatively featureless and, when subtracted from the  $\text{PrP}^{\text{res}}$  spectra (ME7-mock), had little impact on the features of their second-derivative spectra. Another potential complication in comparing the IR spectra of the wild-type and anchorless  $\text{PrP}^{\text{res}}$  preparations is that N-acetylglucosamine moieties in N-linked glycans and GPI anchors can also absorb near the  $\beta$ -sheet region ( $\sim 1638\text{ cm}^{-1}$ ).<sup>4</sup> However, their overall contributions to  $\text{PrP}^{\text{res}}$  spectra in this region should be minor.<sup>4</sup> Indeed, the spectrum of wild-type 22L  $\text{PrP}^{\text{res}}$  was nearly indistinguishable from that of anchorless 22L  $\text{PrP}^{\text{res}}$ , except for



modestly enhanced absorbance centered at  $\sim 1670\text{ cm}^{-1}$  (Figure 7). The latter band is in the spectral region commonly ascribed to turn structures.<sup>39</sup> In the case of ME7 PrP<sup>res</sup>, differences between the wild-type and anchorless structures were subtle, but more apparent than in the 22L PrP<sup>res</sup> preparations. Most notable was a shift in the low-frequency  $\beta$ -sheet band from  $\sim 1620$  to  $\sim 1622\text{ cm}^{-1}$  with the post-translational modifications. Altogether, the IR spectra of anchorless and wild-type PrP<sup>res</sup> provide evidence that the N-linked glycans and GPI anchor do not grossly affect the strain-specific secondary structures of PrP<sup>res</sup> but may have subtle effects on turn (or perhaps loop structures) and, in the case of ME7, certain  $\beta$ -sheet components.

## DISCUSSION

This work provides the first direct evaluation of the effects of the GPI anchor and Asn-linked glycans on PrP<sup>res</sup> conformation. Two recent developments have made these analyses possible: (1) the recent availability of scrapie-infected transgenic mice expressing only anchorless PrP molecules that are also severely deficient in Asn-linked glycans (e.g., see the predominance of the lower, unglycosylated isoform in panels A and B of Figure 2) and (2) our new purification protocols for anchorless and wild-type PrP<sup>res</sup>. These protocols greatly reduce the level of contaminants that, in hindsight, must have confounded previous IR analyses of wild-type murine PrP<sup>res</sup><sup>54</sup> that, notably in the case of 22L PrP<sup>res</sup>, gave spectra that are significantly different than those reported here. Contamination has been much less of a problem with certain hamster PrP<sup>res</sup> preparations because of their much higher starting PrP<sup>res</sup> content per mass of brain tissue. Nevertheless, improvements were observed when the DRM PrP<sup>res</sup> method was applied to hamster 263K PrP<sup>res</sup> as shown by the reduction in the level of ferritin contamination (Figure 3B,D).

Our rationale for purifying wild-type PrP<sup>res</sup> starting with DRM membrane preparations rather than fully detergent-solubilized whole brain homogenates stemmed from the discovery that many contaminants present in preparations made using a standard method<sup>41</sup> seemed to correspond to endogenous brain proteins in mock PrP<sup>res</sup> preparations with biochemical and biophysical properties similar to those of PrP<sup>res</sup>. These properties included detergent insolubility, protease resistance, and high density. Working independently, another group has identified some of the proteins present in both mock and wild-type mouse PrP<sup>res</sup> samples.<sup>46</sup> We reasoned that some of these detergent-insoluble, high-density contaminants might be separated from PrP<sup>res</sup> by floatation of PrP<sup>res</sup>-enriched DRMs on density gradients. To minimize co-enrichment for certain high-molecular mass contaminants such as ferritin due to their direct association with PrP<sup>res</sup> via electrostatic interactions,<sup>40</sup> we subjected the DRM fraction to a high-salt treatment. This should disrupt these interactions and remove these contaminants by recovery of the salt-washed DRMs on a second floatation gradient. The high-salt treatment is a component of a standard PrP<sup>res</sup> purification procedure that is thought to remove some glycosaminoglycans.<sup>41</sup> However, because this treatment is applied to a sarkosyl-extracted brain homogenate, high-density molecules like ferritin that might become dissociated from PrP<sup>res</sup> would still cosediment with the PrP<sup>res</sup> in the subsequent ultracentrifugation step. Because we have found that wild-type PrP<sup>res</sup> of many scrapie strains associates with the DRM fraction, including strains prone to generating large plaquelike PrP<sup>res</sup> deposits [e.g., 87V (data not shown)], it is likely our DRM

PrP<sup>res</sup> purification method can be broadly applied to purification of wild-type GPI-anchored PrP<sup>res</sup>.

Consistent with our rationale, at most very low levels of endogenous brain proteins were enriched in mock anchorless PrP<sup>res</sup> preparations (Figure 2A). The accumulation of anchorless PrP<sup>res</sup> in large amyloid deposits permitted the recovery of anchorless PrP<sup>res</sup> at centrifugation speeds substantially lower than those used for wild-type PrP<sup>res</sup>. This could reduce the opportunity for copurification of high-molecular mass, dense, protease-resistant contaminants (e.g., ferritin). A further modification applied to both the new wild-type and anchorless PrP<sup>res</sup> preparation procedures was the use of Benzonase to digest nucleic acids in place of sequential RNase A and DNase digestions. This avoided the use of RNase A that is partially resistant to PK digestion,<sup>56</sup> forms aggregates under certain conditions,<sup>57,58</sup> and thus could be a source of contamination.

Another group working in parallel has reported the use of DRM fractionation to enrich for PrP<sup>res</sup> with the goal of generating antigen for immunizations to create anti-PrP antisera.<sup>50</sup> Although these authors used DRM fractionation in the initial purification step, subsequent steps to further enrich for PrP<sup>res</sup> were dramatically different from our method. Most importantly, the apparent purity of the PrP<sup>res</sup> from this method was substantially lower than that shown in this study as indicated by the presence of prominent silver-stained bands that were not reactive with anti-PrP antibodies.<sup>50</sup> Moreover, only portions of the gels corresponding to a narrow apparent molecular mass range from  $\sim 20$  to  $50\text{ kDa}$  are shown.<sup>50</sup> Hnasko et al.<sup>50</sup> argue that the lack of induction of antibodies against other brain DRM proteins besides PrP provides evidence of the purity of their PrP<sup>res</sup> preparations. However, this may simply represent murine immunological tolerance to these non-PrP rodent proteins just as they observed for PrP itself (i.e., no anti-hamster PrP antibodies were generated in immunizations of wild-type mice). Although the PrP<sup>res</sup> preparations of Hnasko et al. are useful for immunization experiments, they would not be of sufficient purity for the IR analyses presented here.

Our study strongly reinforces previous reports of the ability of IR spectroscopy to detect differences in conformation between PrP<sup>C</sup> and PrP<sup>res</sup>, as well as between different PrP<sup>res</sup> strains comprised of the same polypeptide precursor.<sup>9–11,39</sup> Relative to those differences, the spectral effects of glycans and GPI anchors on PrP<sup>res</sup> were modest (Figures 5–7). Clearly, differences in  $\beta$ -sheet and apparent turn structures can be resolved between PrP<sup>res</sup> strains of the same amino acid sequence, but there is always potential for spectral overlaps in IR amide I spectra of different polypeptide secondary structures. Thus, an inability to distinguish IR spectra does not guarantee the presence of identical secondary structures, and subtle differences in secondary structures, i.e., involving only a few residues, might also be difficult to detect. Nonetheless, the most straightforward interpretation of these IR data is that glycans and anchors do not cause gross conformational changes that are commensurate with the differences between PrP<sup>res</sup> strains, especially in the case of 22L PrP<sup>res</sup>. A more noticeable effect of these post-translational modifications was seen with the ME7 strain, but much of the spectrum remained unchanged.

Given the apparently tight packing of PrP molecules in PrP<sup>res</sup> fibrils, as evidenced by their resistance to proteinase K digestion and H–D exchange,<sup>42</sup> one can imagine that the presence of bulky post-translational modifications might not only affect monomer conformations but also constrain the options for packing PrP monomers into ordered multimers and amyloid fibrils. Our present data

suggest that the presence of glycans and the GPI anchor do not cause a major restructuring of the underlying polypeptide backbone secondary structures within the 22L and ME7 PrP<sup>res</sup> fibrils. However, the data do not negate the possibility that tertiary and quaternary structures might be affected significantly by glycans and anchors, or that the effects might be more significant with other prion strains.

Recent analyses of the rates of H–D exchange of the polypeptide backbone amide protons in infectious anchorless PrP<sup>res</sup> fibrils have revealed extreme resistance to exchange throughout the entire proteinase K-resistant C-terminal portions of the PrP subunits (i.e., from residues ~80–90 to residue ~223).<sup>42</sup> These results strongly suggest that, contrary to previous IR-based reports,<sup>1,4,5,9</sup> there is virtually no  $\alpha$ -helix in PrP<sup>res</sup>. The previous reports employed different methods of estimating secondary structure compositions from IR spectra that were based on theoretical considerations and empirical calibrations using globular proteins of known structure. However, although such estimates are usually fairly accurate (e.g., ref 59), they may at times be misleading because of ambiguities in band assignments or potential IR distortions due to poorly understood factors such as nonglobularity and/or oligomerization of particular protein samples.<sup>60</sup> In any case, the fact that anchorless PrP<sup>res</sup> appears to lack any of the  $\alpha$ -helices that are present in PrP<sup>C</sup> raises the issue of whether wild-type PrP<sup>res</sup>, with its large hydrophilic glycans attached to Asn residues that are located on, or between, residues comprising helices 2 and 3 in PrP<sup>C</sup>, also lacks those helices. Unfortunately, in the previous studies, the presence of the glycans prevented direct mass spectrometric analysis of H–D exchange in much of the proteinase K-resistant C-terminal region of wild-type PrP<sup>res</sup>.<sup>42</sup> However, the close similarity of the IR spectra of anchorless and fully glycosylated wild-type PrP<sup>res</sup> that we have observed here strongly suggests that they have similar structures. Moreover, the spectra of the wild-type PrP<sup>res</sup> preparations gave no evidence of enhanced  $\alpha$ -helical content that, in PrP<sup>C</sup> and many other proteins, absorb between 1650 and 1657 cm<sup>−1</sup> (Figure 7). Indeed, little, if any, banding in this latter spectral region was observed above the spectral noise for any of the PrP<sup>res</sup> preparations. The adjacent band at 1659 cm<sup>−1</sup> was prominent in anchorless PrP<sup>res</sup> preparations, which we have concluded has no  $\alpha$ -helices; thus, the 1659 cm<sup>−1</sup> band is likely to be due to something other than  $\alpha$ -helix, such as turns. The prominence of the same band in wild-type PrP<sup>res</sup> and the relative lack of bands in the 1650–1657 cm<sup>−1</sup> region lead us to surmise that, like their anchorless counterparts, wild-type 22L and ME7 PrP<sup>res</sup> fibrils have structures comprised predominantly of an extended solvent-inaccessible  $\beta$ -sheet core with occasional turns, but virtually no  $\alpha$ -helix.

## ■ ASSOCIATED CONTENT

**S Supporting Information.** Supporting Figures 1 and 2 as mentioned in the text. This material is available free of charge via the Internet at <http://pubs.acs.org>.

## ■ AUTHOR INFORMATION

### Corresponding Author

\*Phone: (406) 363-9485. Fax: (406) 363-9286. E-mail: [gbaron@niaid.nih.gov](mailto:gbaron@niaid.nih.gov).

### Funding Sources

This research was funded by the Intramural Research Program of the National Institute of Allergy and Infectious Diseases, National Institutes of Health.

## ■ ACKNOWLEDGMENT

Animal experiments were performed in accordance with animal welfare guidelines under an animal study protocol approved by the Animal Care and Use Committee of the Rocky Mountain Laboratories, National Institute of Allergy and Infectious Diseases, National Institutes of Health. We thank Mikael Klingeborn, Roger Moore, and Lara Taubner for critical reading of the manuscript.

## ■ ABBREVIATIONS

CBS, citrate-buffered saline; DRM, detergent-resistant membrane; GPI, glycosylphosphatidylinositol; PK, proteinase K; PrP<sup>C</sup>, normal cellular prion protein; PrP<sup>res</sup>, protease-resistant, disease-associated isoform of prion protein; rPrP, recombinant prion protein; TSE, transmissible spongiform encephalopathy.

## ■ REFERENCES

- (1) Pan, K.-M.; Baldwin, M.; Nguyen, J.; Gasset, M.; Serban, A.; Groth, D.; Mehlhorn, I.; Huang, Z.; Fletterick, R. J.; Cohen, F. E.; and Prusiner, S. B. (1993) Conversion of  $\alpha$ -helices into  $\beta$ -sheet features in the formation of the scrapie prion protein. *Proc. Natl. Acad. Sci. U.S.A.* 90, 10962–10966.
- (2) Riek, R.; Hornemann, S.; Wider, G.; Glockshuber, R.; and Wuthrich, K. (1997) NMR characterization of the full-length recombinant murine prion protein, mPrP(23–231). *FEBS Lett.* 413, 282–288.
- (3) Riek, R.; Hornemann, S.; Wider, G.; Billeter, M.; Glockshuber, R.; and Wuthrich, K. (1996) NMR structure of the mouse prion protein domain PrP(121–231). *Nature* 382, 180–182.
- (4) Caughey, B. W.; Dong, A.; Bhat, K. S.; Ernst, D.; Hayes, S. F.; and Caughey, W. S. (1991) Secondary structure analysis of the scrapie-associated protein PrP 27–30 in water by infrared spectroscopy. *Biochemistry* 30, 7672–7680.
- (5) Gasset, M.; Baldwin, M. A.; Fletterick, R. J.; and Prusiner, S. B. (1993) Perturbation of the secondary structure of the scrapie prion protein under conditions that alter infectivity. *Proc. Natl. Acad. Sci. U.S.A.* 90, 1–5.
- (6) Safar, J.; Roller, P. P.; Gajdusek, D. C.; and Gibbs, C. J., Jr. (1993) Conformational transitions, dissociation, and unfolding of scrapie amyloid (prion) protein. *J. Biol. Chem.* 268, 20276–20284.
- (7) Wuthrich, K.; and Riek, R. (2001) Three-dimensional structures of prion proteins. *Adv. Protein Chem.* 57, 55–82.
- (8) Lee, S.; Antony, L.; Hartmann, R.; Knaus, K. J.; Surewicz, K.; Surewicz, W. K.; and Yee, V. C. (2010) Conformational diversity in prion protein variants influences intermolecular  $\beta$ -sheet formation. *EMBO J.* 29, 251–262.
- (9) Caughey, B.; Raymond, G. J.; and Bessen, R. A. (1998) Strain-dependent differences in  $\beta$ -sheet conformations of abnormal prion protein. *J. Biol. Chem.* 273, 32230–32235.
- (10) Thomzig, A.; Spassov, S.; Friedrich, M.; Naumann, D.; and Beekes, M. (2004) Discriminating scrapie and bovine spongiform encephalopathy isolates by infrared spectroscopy of pathological prion protein. *J. Biol. Chem.* 279, 33847–33854.
- (11) Spassov, S.; Beekes, M.; and Naumann, D. (2006) Structural differences between TSE strains investigated by FT-IR spectroscopy. *Biochim. Biophys. Acta* 1760, 1138–1149.
- (12) Kascak, R. J.; Rubenstein, R.; Merz, P. A.; Carp, R. I.; Wisniewski, H. M.; and Diring, H. (1985) Biochemical differences among scrapie-associated fibrils support the biological diversity of scrapie agents. *J. Gen. Virol.* 66, 1715–1722.
- (13) Kascak, R. J.; Rubenstein, R.; and Carp, R. I. (1991) Evidence for Biological and Structural Diversity Among Scrapie Strains. In *Transmissible Spongiform Encephalopathies: Scrapie, BSE and Related Human Disorders* (Chesebro, B., Ed.) pp 139–152, Springer-Verlag, Berlin.

- (14) Bessen, R. A., and Marsh, R. F. (1992) Biochemical and physical properties of the prion protein from two strains of transmissible mink encephalopathy agent. *J. Virol.* 66, 2096–2101.
- (15) Bessen, R. A., and Marsh, R. F. (1994) Distinct PrP properties suggest the molecular basis of strain variation in transmissible mink encephalopathy. *J. Virol.* 68, 7859–7868.
- (16) Bessen, R. A., Kocisko, D. A., Raymond, G. J., Nandan, S., Lansbury, P. T., Jr., and Caughey, B. (1995) Nongenetic propagation of strain-specific phenotypes of scrapie prion protein. *Nature* 375, 698–700.
- (17) Parchi, P., Castellani, R., Capellari, S., Ghetti, B., Young, K., Chen, S. G., Farlow, M., Dickson, D. W., Sima, A. A. F., Trojanowski, J. Q., Petersen, R. B., and Gambetti, P. (1996) Molecular basis of phenotypic variability in sporadic Creutzfeldt-Jakob disease. *Ann. Neurol.* 39, 767–778.
- (18) Collinge, J., Sidle, K. C. L., Meads, J., Ironside, J., and Hill, A. F. (1996) Molecular analysis of prion strain variation and the aetiology of “new variant” CJD. *Nature* 383, 685–690.
- (19) Safar, J., Wille, H., Itri, V., Groth, D., Serban, H., Torchia, M., Cohen, F. E., and Prusiner, S. B. (1998) Eight prion strains have PrP(Sc) molecules with different conformations. *Nat. Med.* 4, 1157–1165.
- (20) Fernie, K., Steele, P. J., Taylor, D. M., and Somerville, R. A. (2007) Comparative studies on the thermostability of five strains of transmissible-spongiform-encephalopathy agent. *Biotechnol. Appl. Biochem.* 47, 175–183.
- (21) Wille, H., Michelitsch, M. D., Guenebaut, V., Supattapone, S., Serban, A., Cohen, F. E., Agard, D. A., and Prusiner, S. B. (2002) Structural studies of the scrapie prion protein by electron crystallography. *Proc. Natl. Acad. Sci. U.S.A.* 99, 3563–3568.
- (22) Wille, H., Govaerts, C., Borovinskiy, A., Latawiec, D., Downing, K. H., Cohen, F. E., and Prusiner, S. B. (2007) Electron crystallography of the scrapie prion protein complexed with heavy metals. *Arch. Biochem. Biophys.* 467, 239–248.
- (23) Sim, V. L., and Caughey, B. (2009) Ultrastructures and strain comparison of under-glycosylated scrapie prion fibrils. *Neurobiol. Aging* 30, 2031–2042.
- (24) Caughey, B., Race, R. E., Ernst, D., Buchmeier, M. J., and Chesebro, B. (1989) Prion protein (PrP) biosynthesis in scrapie-infected and uninfected neuroblastoma cells. *J. Virol.* 63, 175–181.
- (25) Hay, B., Barry, R. A., Lieberburg, I., Prusiner, S. B., and Lingappa, V. R. (1987) Biogenesis and transmembrane orientation of the cellular isoform of the scrapie prion protein. *Mol. Cell. Biol.* 7, 914–920.
- (26) Stahl, N., Borchelt, D. R., Hsiao, K., and Prusiner, S. B. (1987) Scrapie prion protein contains a phosphatidylinositol glycolipid. *Cell* 51, 229–240.
- (27) Vorberg, I., and Priola, S. A. (2002) Molecular basis of scrapie strain glycoform variation. *J. Biol. Chem.* 277, 36775–36781.
- (28) Neuendorf, E., Weber, A., Saalmueller, A., Schatzl, H., Reifenberg, K., Pfaff, E., and Groschup, M. H. (2004) Glycosylation deficiency at either one of the two glycan attachment sites of cellular prion protein preserves susceptibility to bovine spongiform encephalopathy and scrapie infections. *J. Biol. Chem.* 279, 53306–53316.
- (29) Tuzi, N. L., Cancellotti, E., Baybutt, H., Blackford, L., Bradford, B., Plinston, C., Coghill, A., Hart, P., Piccardo, P., Barron, R. M., and Manson, J. C. (2008) Host PrP glycosylation: A major factor determining the outcome of prion infection. *PLoS Biol.* 6, e100.
- (30) Cancellotti, E., Bradford, B. M., Tuzi, N. L., Hickey, R. D., Brown, D., Brown, K. L., Barron, R. M., Kisielewski, D., Piccardo, P., and Manson, J. C. (2010) Glycosylation of PrP<sup>C</sup> determines timing of neuroinvasion and targeting in the brain following transmissible spongiform encephalopathy infection by a peripheral route. *J. Virol.* 84, 3464–3475.
- (31) Lawson, V. A., Priola, S. A., Wehrly, K., and Chesebro, B. (2001) N-terminal truncation of prion protein affects both formation and conformation of abnormal protease-resistant prion protein generated in vitro. *J. Biol. Chem.* 276, 35265–35271.
- (32) Winkhofer, K. F., Heller, U., Reintjes, A., and Tatzelt, J. (2003) Inhibition of complex glycosylation increases the formation of PrP<sup>Sc</sup>. *Traffic* 4, 313–322.
- (33) Piro, J. R., Harris, B. T., Nishina, K., Soto, C., Morales, R., Rees, J. R., and Supattapone, S. (2009) Prion protein glycosylation is not required for strain-specific neurotropism. *J. Virol.* 83, 5321–5328.
- (34) Chesebro, B., Trifilo, M., Race, R., Meade-White, K., Teng, C., LaCasse, R., Raymond, L., Favara, C., Baron, G., Priola, S., Caughey, B., Masliah, E., and Oldstone, M. (2005) Anchorless prion protein results in infectious amyloid disease without clinical scrapie. *Science* 308, 1435–1439.
- (35) Chesebro, B., Race, B., Meade-White, K., LaCasse, R., Race, R., Klingeborn, M., Striebel, J., Dorward, D., McGovern, G., and Jeffrey, M. (2010) Fatal transmissible amyloid encephalopathy: A new type of prion disease associated with lack of prion protein membrane anchoring. *PLoS Pathog.* 6, e1000800.
- (36) Klingeborn, M., Race, B., Meade-White, K. D., Rosenke, R., Striebel, J. F., and Chesebro, B. (2011) Crucial Role for Prion Protein Membrane Anchoring in the Neuroinvasion and Neural Spread of Prion Infection. *J. Virol.* 85, 1484–1494.
- (37) Kocisko, D. A., Come, J. H., Priola, S. A., Chesebro, B., Raymond, G. J., Lansbury, P. T., and Caughey, B. (1994) Cell-free formation of protease-resistant prion protein. *Nature* 370, 471–474.
- (38) Walmsley, A. R., Zeng, F., and Hooper, N. M. (2001) Membrane topology influences N-glycosylation of the prion protein. *EMBO J.* 20, 703–712.
- (39) Beekes, M., Lasch, P., and Naumann, D. (2007) Analytical applications of Fourier transform-infrared (FT-IR) spectroscopy in microbiology and prion research. *Vet. Microbiol.* 123, 305–319.
- (40) Mishra, R. S., Basu, S., Gu, Y., Luo, X., Zou, W. Q., Mishra, R., Li, R., Chen, S. G., Gambetti, P., Fujioka, H., and Singh, N. (2004) Protease-resistant human prion protein and ferritin are cotransported across Caco-2 epithelial cells: Implications for species barrier in prion uptake from the intestine. *J. Neurosci.* 24, 11280–11290.
- (41) Raymond, G. J., and Chabry, J. (2004) Purification of the pathological isoform of prion protein (PrP<sup>Sc</sup> or PrP<sup>Pres</sup>) from transmissible spongiform encephalopathy-affected brain tissue. In *Techniques in Prion Research* (Lehmann, S., and Grassi, J., Eds.) pp 16–26, Birkhauser Verlag, Basel, Switzerland.
- (42) Smirnovas, V., Baron, G. S., Offerdahl, D. K., Raymond, G. J., Caughey, B., and Surewicz, W. K. (2011) Structural organization of brain-derived mammalian prions examined by hydrogen-deuterium exchange. *Nat. Struct. Mol. Biol.* 18, 504–506.
- (43) Blum, H., Beier, H., and Gross, H. J. (1987) Improved silver staining of plant proteins, RNA and DNA in polyacrylamide gels. *Electrophoresis* 8, 93–99.
- (44) Atarashi, R., Wilham, J. M., Christensen, L., Hughson, A. G., Moore, R. A., Johnson, L. M., Onwubiko, H. A., Priola, S. A., and Caughey, B. (2008) Simplified ultrasensitive prion detection by recombinant PrP conversion with shaking. *Nat. Methods* 5, 211–212.
- (45) Race, B., Meade-White, K., Oldstone, M. B., Race, R., and Chesebro, B. (2008) Detection of prion infectivity in fat tissues of scrapie-infected mice. *PLoS Pathog.* 4, e1000232.
- (46) Moore, R. A., Timmes, A., Wilmarth, P. A., and Priola, S. A. (2010) Comparative profiling of highly enriched 22L and Chandler mouse scrapie prion protein preparations. *Proteomics* 10, 2858–2869.
- (47) Russelakis-Carneiro, M., Hetz, C., Maundrell, K., and Soto, C. (2004) Prion replication alters the distribution of synaptophysin and caveolin 1 in neuronal lipid rafts. *Am. J. Pathol.* 165, 1839–1848.
- (48) Naslavsky, N., Stein, R., Yanai, A., Friedlander, G., and Taraboulos, A. (1997) Characterization of detergent-insoluble complexes containing the cellular prion protein and its scrapie isoform. *J. Biol. Chem.* 272, 6324–6331.
- (49) Meier, P., Genoud, N., Prinz, M., Maissen, M., Rulicke, T., Zurbriggen, A., Raeber, A. J., and Aguzzi, A. (2003) Soluble dimeric prion protein binds PrP<sup>Sc</sup> in vivo and antagonizes prion disease. *Cell* 113, 49–60.
- (50) Hnasko, R., Serban, A. V., Carlson, G., Prusiner, S. B., and Stanker, L. H. (2010) Generation of antisera to purified prions in lipid rafts. *Prion* 4, 94–104.
- (51) Madore, N., Smith, K. L., Graham, C. H., Jen, A., Brady, K., Hall, S., and Morris, R. (1999) Functionally different GPI proteins are



organized in different domains on the neuronal surface. *EMBO J.* 18, 6917–6926.

(52) Chen, X., Jen, A., Warley, A., Lawrence, M. J., Quinn, P. J., and Morris, R. J. (2009) Isolation at physiological temperature of detergent-resistant membranes with properties expected of lipid rafts: The influence of buffer composition. *Biochem. J.* 417, 525–533.

(53) Taylor, C. M., Coetzee, T., and Pfeiffer, S. E. (2002) Detergent-insoluble glycosphingolipid/cholesterol microdomains of the myelin membrane. *J. Neurochem.* 81, 993–1004.

(54) Atarashi, R., Sim, V. L., Nishida, N., Caughey, B., and Katamine, S. (2006) Prion strain-dependent differences in conversion of mutant prion proteins in cell culture. *J. Virol.* 80, 7854–7862.

(55) Callahan, M. A., Xiong, L., and Caughey, B. (2001) Reversibility of scrapie-associated prion protein aggregation. *J. Biol. Chem.* 276, 28022–28028.

(56) Rauber, N. R., Jany, K. D., and Pfeleiderer, G. (1978) Ribonuclease A digestion by proteinase K. *Z. Naturforsch. C33*, 660–663.

(57) Townsend, M. W., and DeLuca, P. P. (1990) Stability of ribonuclease A in solution and the freeze-dried state. *J. Pharm. Sci.* 79, 1083–1086.

(58) Libonati, M., and Gotte, G. (2004) Oligomerization of bovine ribonuclease A: Structural and functional features of its multimers. *Biochem. J.* 380, 311–327.

(59) Dong, A., Huang, P., and Caughey, W. S. (1990) Protein secondary structures in water from second-derivative amide I infrared spectra. *Biochemistry* 29, 3303–3308.

(60) Surewicz, W. K., Mantsch, H. H., and Chapman, D. (1993) Determination of protein secondary structure by Fourier transform infrared spectroscopy: A critical assessment. *Biochemistry* 32, 389–394.